

Law of the wall in an unstably stratified turbulent channel flow

A. SCAGLIARINI^{1,2,3} H. EINARSSON²
A. GYLFASON² F. TOSCHI^{3,4,5}

¹ Department of Physics and INFN, University of Rome “Tor Vergata”, Via della Ricerca Scientifica 1, 00133 Rome, Italy

² School of Science and Engineering, Reykjavik University, Menntavegur 1, IS-101 Reykjavik, Iceland

³ Department of Mathematics and Computer Science, Eindhoven University of Technology, The Netherlands

⁴ Department of Applied Physics, Eindhoven University of Technology, The Netherlands

⁵ IAC-CNR, Via dei Taurini 19, 00185 Rome, Italy

(Received Nov 1, 2014)

We perform direct numerical simulations of an unstably stratified turbulent channel flow to address the effects of buoyancy on the boundary layer dynamics and mean field quantities. We systematically span a range of parameters in the space of friction Reynolds number (Re_τ) and Rayleigh number (Ra). Our focus is on deviations from the logarithmic law of the wall due to buoyant motion. The effects of convection in the relevant ranges are discussed providing measurements of mean profiles of velocity, temperature and Reynolds stresses as well as of the friction coefficient. A phenomenological model is proposed and shown to capture the observed deviations of the velocity profile in the log-law region from the non-convective case.

1. Introduction

Wall bounded turbulence is highly relevant to a variety of engineering systems and naturally occurring flows. As such, the importance of the fundamental understanding of the generation of turbulent fluctuations by fluid-solid interactions in the boundary layers and their transport and interaction with the bulk mean flow (Pope 2001) is evident. In many geophysical and industrial flows, shear flows and wall turbulence are subjected to either stable or unstable thermal stratifications. Stable stratification is known to inhibit the bursting phenomenon, i.e. depleting the transport of turbulent fluctuations from the wall to the bulk, thus reducing the turbulent drag and increasing the mean flow velocity. Many studies have been devoted to this situation when the stratified scalar field is passive (Johansson & Wikström 1999; Papavassiliou & Hanratty 1997) and active (Armenio & Sarkar 2002; Gerz, Schumann & Elgobashi 1989; Iida, Kasagi & Nagano 2002; García-Villalba & del Álamo 2011) and even in presence of non-Oberbeck-Boussinesq effects (Zonta, Onorato & Soldati 2012).

The unstable configuration is also relevant in a variety of instances, such as the physics of the atmospheric surface layer superposed to an over-heated ground (as, e.g., in summer days, determining the generation of thermo-convective storms (Bluestein 2013)); when buoyancy forces are strong enough, thermal convection can occur, altering significantly the unstable boundary layer dynamics. Early theoretical results on turbulent boundary layers under unstable thermal stratification date back to Prandtl (1932) who pioneered a mixing-length based approach which inspired the later work of Obukhov (1946) anticipating the Monin-Obukhov similarity theory (Monin & Obukhov 1954), and subsequently revised and compared with experimental data by Kader & Yaglom (1990). Lumley, Zeman & Siess (1978) proposed an eddy-damped quasi-Gaussian closure able to predict the inversion regions of heat flux profiles in strongly buoyant

sheared boundary layers. Numerical results (Iida & Kasagi 1997) and experimental flume measurements (combined with a spectral equation model) (Komori *et al* 1982) showed that natural thermal convection affects the mechanisms of momentum and heat transport from the wall and tends to flatten the velocity profile in the bulk; these observation were confirmed by large-eddy simulations of a variable density fluid (Zainali & Lessani 2010), although with non-Boussinesq effects, as, e.g. profile asymmetries emerging at large stratifications.

In this work we perform direct numerical simulations based on the lattice Boltzmann (hereafter LB) method of an unstably (thermally) stratified turbulent channel flow. Our focus is on identifying the effects of buoyancy on the channel flow structure by comparing profiles of mean fields and fluctuations over a wide range of parameters with a pure (unstratified) channel flow. Our results show a decreased fluid throughput due to a strongly flattened velocity profile, which could, however, be fitted by a log-law with coefficients depending on the input controlling parameters (friction Reynolds number Re_τ and Rayleigh number Ra , defined below), as also derived theoretically.

2. Numerical method and simulation details

We simulated a fluid enclosed between two walls, kept at fixed temperatures T_H at $y = 0$ and $T_C = T_H - \Delta$ at $y = 2H$, and driven by a constant pressure gradient p' along the streamwise direction \hat{x} (see figure 1). The equations of motion are the incompressible Navier-Stokes equation for the fluid velocity field $\mathbf{u}(\mathbf{x}, t)$ in the Boussinesq approximation (namely, the density is assumed to be constant $\rho = \rho_0$, but for the linearised buoyancy term)

$$\partial_t \mathbf{u} + \mathbf{u} \cdot \nabla \mathbf{u} = -\nabla P + \nu \Delta \mathbf{u} - \beta \mathbf{g}(T - T_m) + \mathbf{F}, \quad (2.1)$$

($T_m = (T_H + T_C)/2$ being the mean temperature) coupled with the advection-diffusion equation for the temperature field $T(\mathbf{x}, t)$

$$\partial_t T + \mathbf{u} \cdot \nabla T = \alpha \Delta T. \quad (2.2)$$

In the above equations, P is the fluctuating pressure field (rescaled by ρ_0), $\mathbf{g} = -g\hat{y}$ the acceleration of gravity, $\mathbf{F} = p'\hat{x}$ a constant acceleration due to the imposed pressure head p' ; ν , α and β are the kinematic viscosity, the thermal diffusivity and thermal expansion coefficient, respectively. As a numerical scheme, we adopted a 3d LB algorithm (Benzi, Succi & Vergassola 1992; Chen & Doolen 1998; Aidun & Clausen 2010) with two probability densities (for density/momentum and for temperature, respectively) (He, Chen & Doolen 1998). In such mesoscopic model the fluid is described by a discrete kinetic distribution function $f_i(\mathbf{r}, \mathbf{c}_i, t)$ which measures the probability of finding a molecule at position \mathbf{r} at time t and with a velocity \mathbf{c}_i that can take only a finite number of possible values (specifically, our lattice scheme features nineteen speeds). The distribution functions evolve in time according to a discrete version of the Boltzmann equation, which algorithmically corresponds to a sequence of free-streaming and two-body collisions steps, the latter being described by a relaxation towards a local equilibrium ($f_i^{(eq)}$) with a characteristic time τ_{LB} :

$$f_i(\mathbf{r} + \mathbf{c}_i \Delta t, \mathbf{c}_i, t + \Delta t) - f_i(\mathbf{r}, \mathbf{c}_i, t) = -\frac{1}{\tau_{LB}} \left(f_i(\mathbf{r}, \mathbf{c}_i, t) - f_i^{(eq)}(\mathbf{r}, \mathbf{c}_i, t) \right) + \mathcal{S}_i^{(tot)}(\mathbf{r}, \mathbf{c}_i, t), \quad (2.3)$$

where $\mathcal{S}_i^{(tot)}$ is a source term: such term produces the desired total force $\mathcal{F}^{(tot)}$ (including the buoyancy term and the driving due to the pressure gradient) once it is projected on the momentum field, i.e. $\sum_i \mathcal{S}_i^{(tot)} \mathbf{c}_i = \mathcal{F}^{(tot)}$. Local equilibria are given by the following low Mach number,

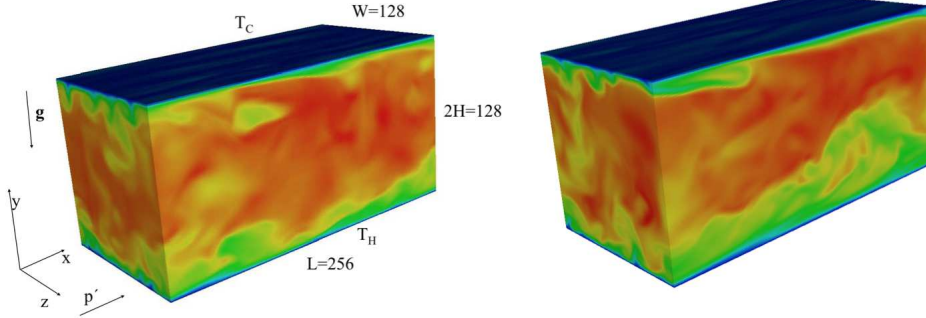


FIGURE 1. Snapshots of the streamwise velocity field in the simulation domain (color map: velocity in the range $[0; 20u_\tau]$ from blue to red) for $Re_\tau = 205$ and $Ra = 0$ (left) and $Ra = 6.5 \times 10^6$ (right). The physical domain is also displaced along with the coordinate system adopted in the text.

Ma , expansion of the Maxwellian distribution

$$f_i^{(eq)} = w_i \rho \left[1 + \frac{\mathbf{u} \cdot \mathbf{c}_i}{c_s^2} + \frac{\mathbf{u}\mathbf{u} : (\mathbf{c}_i \mathbf{c}_i - c_s^2 \mathbf{I})}{2c_s^4} \right], \quad (2.4)$$

where w_i is a set of weights chosen in such a way to maximize the algebraic degree of precision in the computation of the hydrodynamic fields and $c_s = 1/\sqrt{3}$ constant of the model (representing the speed of sound). In all the regimes spanned by our simulations $Ma \ll 1$, so that the system behaves as incompressible although the divergence-free condition is not explicitly imposed.

In the small Knudsen number limit, the integration of (2.3) (coupled with an analogous equation for the temperature dynamics) solves numerically equations (2.1) and (2.2) (Wolf-Gladrow 2001) for the coarse-grained hydrodynamical fields defined as $\mathbf{u} = \sum_i \mathbf{c}_i f_i$ and $T = \sum_i g_i$, where g_i is a set of auxiliary distribution functions for the temperature equation; the transport coefficient of Navier-Stokes and temperature equations (i.e. the viscosity ν and thermal diffusivity α) are related to the relaxation times of the respective LB equations through $\nu = c_s^2(\tau_{LB} - 1/2)$ and $\alpha = c_s^2(\tau_{LB}^{(T)} - 1/2)$ ($\tau_{LB}^{(T)}$ being the relaxation time of the LB equation for the g_i 's), where c_s is the speed of sound.

The numerical method has been extensively used to study both thermal convection (Benzi, Toschi & Tripiccione 1998; Calzavarini, Toschi & Tripiccione 2002) and turbulent channel flow (Toschi *et al* 1999; Toschi, L ev eque & Ruiz-Chavarr a 2000; Biferale *et al* 2002); in particular Lavezzo, Clercx & Toschi (2011) validated the code and tested grid resolutions against previous studies with different numerical methods.

We used a computational grid $L \times 2H \times W$ of $256 \times 128 \times 128$ lattice points, with each run longer than 3×10^6 time steps (in LB units), in such a way to achieve statistically steady states of $\sim 200T_L$ (T_L being the large-scale eddy turnover time). The domain under consideration is sketched in figure 1, where a snapshot of an instantaneous u_x field is shown.

From equations (2.1) and (2.2) two dimensionless groups can be identified giving rise to two parameters which control the dynamics, namely the shear (or friction) Reynolds number,

$$Re_\tau = \frac{u_\tau H}{\nu}$$

($u_\tau = \sqrt{p'H}$ being the friction velocity) and the Rayleigh number

$$Ra = \frac{\beta g \Delta (2H)^3}{\nu \alpha}$$

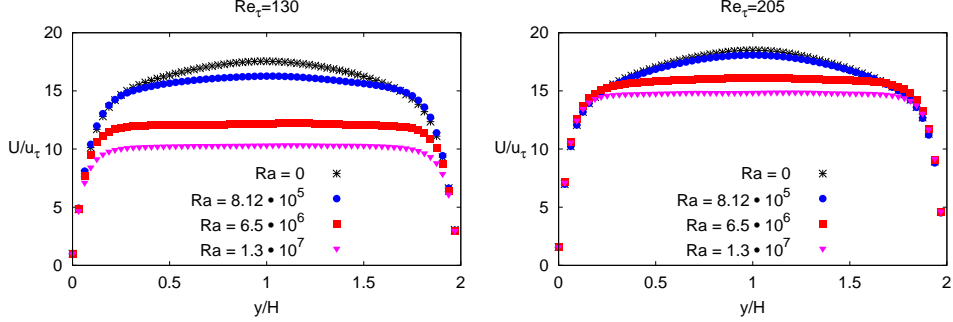


FIGURE 2. Mean profiles of the streamwise velocity $U(y)$, normalized with the friction velocity u_τ , for various Rayleigh numbers ($Ra = 0$, $Ra = 8.12 \times 10^5$, $Ra = 6.5 \times 10^6$ and $Ra = 1.3 \times 10^7$) at fixed shear Reynolds number Re_τ . Left: $Re_\tau = 130$, Right: $Re_\tau = 205$.

quantifying, respectively, the strength of the pressure induced shear and of the buoyancy with respect to viscous dissipation.

We performed turbulent channel flow simulations with $Re_\tau \in [46, 205]$; for each Re_τ we tuned the gravity (at fixed temperature jump), whence the buoyancy, spanning the range $Ra \in [0, 1.3 \times 10^7]$.

3. Results

Mean profiles of the streamwise velocity $U(y) = \overline{u_x}$ (the overline indicates here and henceforth averaging over planes parallel to the walls $\overline{(\cdot)} = (L_x L_z)^{-1} \int (\cdot) dx dz$ in the channel) are shown in Figure 2. For each Reynolds number ($Re_\tau = 130$ and $Re_\tau = 205$) we show data from simulations at three different Rayleigh numbers ($Ra = 8.12 \times 10^5$, $Ra = 6.5 \times 10^6$ and $Ra = 1.3 \times 10^7$), besides the unstratified channel flow ($Ra = 0$). An evident effect of thermal stratification is a decrease of the centreline velocity and a flattening of the profiles at increasing Ra ; indeed, mixing between the bulk and the boundary layer regions due to wall-normal thermal fluctuations (or “plumes”) results in an increase of the effective wall drag (Hattori, Morita & Nagano 2006). Such effects are more pronounced for lower Re_τ , as it clearly appears by comparison of left and right panels of figure 2. These observations will be discussed more quantitatively under the light of the modelling in the next section.

Figure 3 shows the mean temperature profile with respect to y , for the same cases displayed in Figure 2. Here, we note the bending of the thermal profile in the bulk with increased Reynolds number, in contrast to the thermal shortcut observed in pure Rayleigh-Bénard (at sufficiently high Rayleigh numbers) (Scagliarini, Gylfason & Toschi 2014), owing to the destruction or sweeping of the coherent plumes rising from the wall surfaces.

Longitudinal and transverse mean squared components of the fluctuating velocity field (hereafter $\tilde{u}_i = u_i - \overline{u}_i$) are shown in Figure 4 for the same cases as in Figure 2 (normalized with the friction velocity). When the fluctuating quantities are concerned, most notably the lateral component is increased in the bulk region, and as the Rayleigh number is increased, the magnitude becomes comparable or greater than the stream-wise component. The near wall regions are also affected, primarily in the streamwise component, where an increase and a subsequent decrease in magnitude is observed as the Rayleigh number is increased.

In order to quantify the overall effect of the thermal forcing on the channel flow, figure 5 shows the skin-friction coefficient $c_f = \tau_w / (1/2 U_0^2)$ as a function of shear Reynolds number Re_τ . The increased drag due to the thermal field is evident, resulting in higher than usual friction coefficient. The effect is reduced asymptotically, as the Reynolds number is increased for a

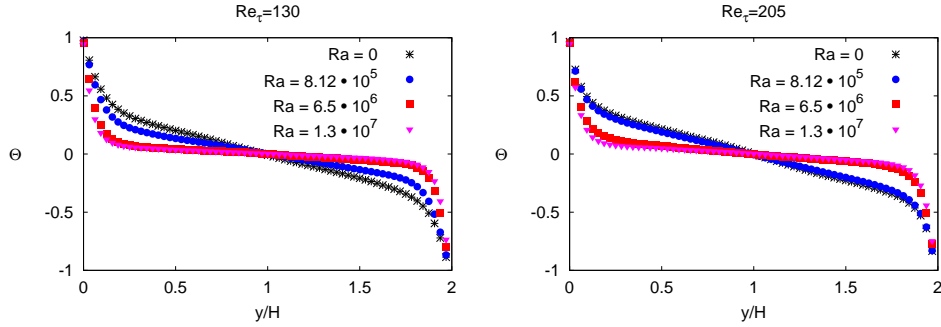


FIGURE 3. Mean profiles of the normalized temperature $\Theta = 2(T - T_m)/\Delta$ as a function of the height y for various Rayleigh numbers ($Ra = 0$, $Ra = 8.12 \times 10^5$, $Ra = 6.5 \times 10^6$ and $Ra = 1.3 \times 10^7$) at fixed shear Reynolds number Re_τ . Left: $Re_\tau = 130$, Right: $Re_\tau = 205$.

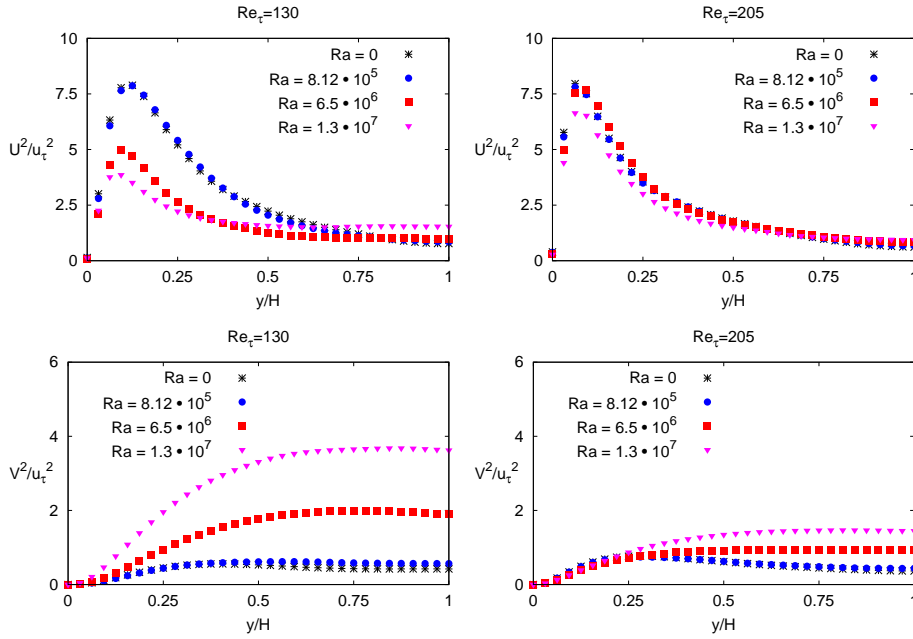


FIGURE 4. Profiles of longitudinal $U^2 = \overline{u_x^2}$ and transverse $V^2 = \overline{u_y^2}$ mean squared components of the fluctuating velocity field, normalized by the friction velocity u_τ for various Rayleigh numbers ($Ra = 0$, $Ra = 8.12 \times 10^5$, $Ra = 6.5 \times 10^6$ and $Ra = 1.3 \times 10^7$) at fixed shear Reynolds number Re_τ .

given Rayleigh number, emphasizing that shear becomes the dominant source of turbulence at sufficiently high Reynolds numbers.

4. Modification of the law of the wall by buoyancy

Inspection of the profiles of the mean quantities and the fluctuations showed that buoyancy alters the channel flow structure. We now focus on the mean velocity profiles. In Figure 6 we report the lin-log plot of profiles, in wall units, for $Re_\tau = 185$ and for various Ra . Convective motion, realised in the form of thermal plumes rising from the walls to the bulk, disturbs the coherence of the channel flow, resulting in a source of drag which decreases the mean velocity in the channel and hence the mass throughput, as well as flattening the velocity profile.

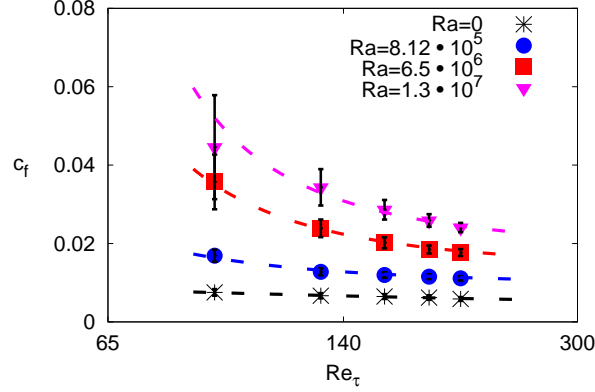


FIGURE 5. The skin-friction coefficient $c_f = \tau_w / (1/2U_0^2)$ as a function of the shear Reynolds number Re_τ for various Rayleigh numbers Ra . The dashed lines are predictions obtained by approximating the mean velocity by a log-law over the whole channel; for the stratified cases we made use of equations (4.1)-(4.2) with the same fitting parameter $C_s = 2.5$ for all Ra (see section 4.)

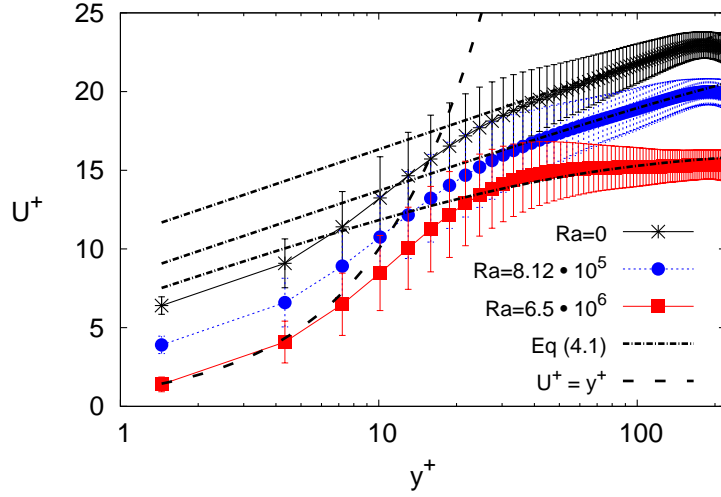


FIGURE 6. Lin-log plot of the velocity profiles in wall units, for shear Reynolds number $Re_\tau = 185$ (left panel) and Rayleigh numbers $Ra = 0$ (*), $Ra = 8.12 \times 10^5$ (●) and $Ra = 6.5 \times 10^6$ (■). The dashed lines indicate the linear law, valid in the viscous layer, $U^+ = y^+$, while the dash-dotted ones correspond to the prediction (4.1)-(4.2) with $\kappa = 0.42$, $C_s = 2.5$ and $B \in [5.8, 6.7]$ ($Pr = 1$).

In order to quantify these observations, in the following we attempt to generalize von Kármán's law of the wall accounting for buoyancy effects. To this aim, we propose a simple model constructed from conservation laws and phenomenological arguments, which predicts that the viscous buffer is insensitive to buoyancy (i.e. $U^+ = y^+$), while in the log-law region the following relation

$$U^+(y^+) = \kappa^{-1} \log \left(\frac{y^+}{1 + \kappa_C y^+} \right) + B, \quad (4.1)$$

holds (quantities have been expressed in wall units $U^+ \equiv U/u_\tau$ and $y^+ \equiv y/\delta$, with $\delta = \nu/u_\tau$).

In equation (4.1), κ is the von Kármán constant, B is an integration constant and κ_C is given by

$$\kappa_C(Ra, Re_\tau) = C_S \frac{Ra}{Re_\tau^4 Pr^2}; \quad (4.2)$$

C_S is a phenomenological parameter. All profiles in Figure 6 agree with our predictions: all curves collapse on the function $U^+ = y^+$ for $y^+ < 10$ (dashed lines) while in the logarithmic layer they can be fitted with equation (4.1) (dash-dotted lines), whose derivation is detailed in what follows.

Applying the Reynolds decomposition $\mathbf{u}(\mathbf{x}, t) = U(y)\hat{x} + \tilde{\mathbf{u}}(\mathbf{x}, t)$ for the velocity field and averaging the Navier-Stokes equation for the \hat{x} velocity component, we get, upon integration in y , an exact relation (Pope 2001) between the mean shear $S(y) = dU(y)/dy$ and the Reynolds stress $\tau_{xy}(y) = -\overline{\tilde{u}_x \tilde{u}_y}$ namely:

$$\nu S(y) + \tau_{xy}(y) = p'(H - y), \quad (4.3)$$

or, in wall units:

$$S^+(y^+) + \tau_{xy}^+(y^+) = \left(1 - \frac{y^+}{Re_\tau}\right). \quad (4.4)$$

Notice that equations (4.3)-(4.4) remain valid also in the presence of buoyancy, since the forcing term $\beta g(T - T_m)\hat{y}$ does not act along the streamwise direction. For very large Re_τ (in principle $Re_\tau \rightarrow \infty$), equation (4.4) gives $S^+ + \tau_{xy}^+ = 1$; close to the wall (for $y^+ < 10$), then, where viscous terms dominate, $S^+ \ll \tau_{xy}^+$ whence $S^+ \approx 1$ which implies $U^+ \simeq y^+$, as anticipated above. Conversely, away from the wall (typically for $y^+ \gtrsim 30$), turbulent fluctuations dominate over viscous processes and $\tau_{xy}^+ \ll S^+$, i.e. (L'vov *et al* 2004)

$$\tau_{xy}^+ \approx const; \quad (4.5)$$

such result alone, however, does not give any further insight on the behaviour of the velocity profile in the corresponding region of the channel. To this aim, we need to consider the budget equation of turbulent kinetic energy $E_K(y) = |\tilde{\mathbf{u}}|^2/2$ (Pope 2001). In the log-law layer the energy production $\mathcal{P} = \tau_{xy}(y)S(y) + \beta g\phi(y)$ is balanced by dissipation $\varepsilon(y) = 2\nu(\partial_i \tilde{u}_j)^2$ (Pope 2001); the latter cannot be calculated exactly but only inferred by means of phenomenological arguments: for large Reynolds number and outside the viscous boundary layer, the dissipation equals the turbulent energy flux, which can be estimated as $E_K(y)/\tau(y)$, where $\tau(y) \propto y/\sqrt{E_K(y)}$ is the typical eddy turn-over time at y (L'vov *et al* 2004). Thus, the energy balance equation reads:

$$\frac{aE_K^{3/2}(y)}{y} = \tau_{xy}(y)S(y) + \beta g\phi(y), \quad (4.6)$$

where a is a non-dimensional parameter of order unity.

Equation (4.6) is not yet closed: a relation between $E_K(y)$ and $\tau_{xy}(y)$ is required. Dimensional analysis suggests that the two quantities should be proportional to each other, i.e. $E_K(y) \propto \tau_{xy}(y)$ (L'vov *et al* 2004); such assumption can be readily tested in the numerical simulations: in the main panel of Figure 7 we show that the ratio $E_K(y)/\tau_{xy}(y)$, indeed, approaches a constant value for $y^+ \gtrsim 40$. Equation (4.6) can be then rewritten as (in view also of (4.5))

$$\frac{a(E_K)^{3/2}}{y} = cE_K S(y) + \beta g\phi(y), \quad (4.7)$$

with c yet another dimensionless number. The energy production by buoyancy term, viz. the heat flux, needs also to be modelled; although more refined closures can be employed (Johansson & Wikström

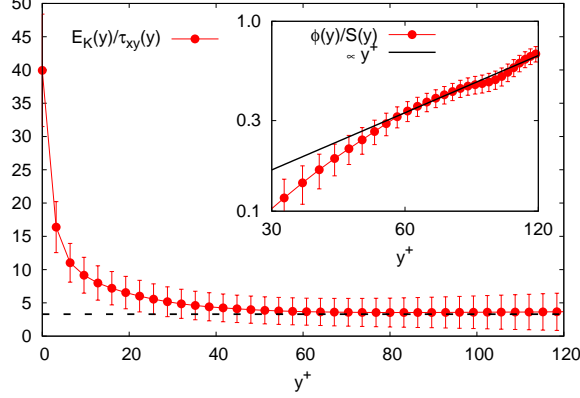


FIGURE 7. Main panel: Ratio of the turbulent kinetic energy E_K over the Reynolds stress τ_{xy} : the plateau attained for $y^+ \gtrsim 40$ suggests that the two quantities are proportional to each other in the log-law region. Inset: Ratio of the turbulent heat flux over the mean shear; the solid line indicates a linear dependence on y^+ and represents a numerical check of the validity of the assumptions leading to equation (4.11).

1999; Hattori, Morita & Nagano 2006) involving tensorial eddy diffusivities and coupling with gradients of the temperature field in all directions, we adopt a simple standard mixing length *ansatz*, i.e.

$$\phi(y) = \overline{u_y \theta} = -\ell_m^2 \partial_y \overline{U} \partial_y \overline{T}. \quad (4.8)$$

A first order closure like (4.8) must not be expected to work well for second order quantities like temperature fluctuations, Reynolds stresses, etc, but, as we will show, mean streamwise velocity profiles are satisfactorily reproduced through such model; according to Prandtl's hypothesis the mixing length ℓ_m is proportional to the distance from the wall, i.e. $\ell_m \propto y$, whence

$$\phi(y) = \overline{u_y \theta} = -by^2 \partial_y \overline{U} \partial_y \overline{T}, \quad (4.9)$$

where b is a numerical constant. The mean temperature gradient will, in principle, depend itself on the shear profile; however, in a perturbative spirit, we postulate here, for simplicity, a logarithmic form, such that

$$\frac{d\overline{T}}{dy} = -\frac{T_*}{y}, \quad (4.10)$$

where $T_* = \frac{\alpha \Delta}{2H u_\tau}$ is a scale for the dynamic temperature. The form (4.10) somehow interpolates between the passive scalar case Johansson & Wikström (1999) and the natural convection Ahlers *et al* (2012); inserted in the expression for the heat flux (4.9) it gives

$$\phi(y) \propto by^2 S(y) \frac{T_*^{(C)}}{y} = b'y S(y) T_*^{(C)}. \quad (4.11)$$

For the sake of validation of our arguments, we check equation (4.11) (which predicts $\phi(y) \propto yS(y)$) against the numerics in the inset of Figure 7, finding a reasonably good agreement. Inserting (4.11) into (4.7) provides

$$\frac{a(E_K)^{3/2}}{y} = cE_K S(y) + \beta g b' y S(y) \frac{\alpha \Delta}{2H u_\tau},$$

which can be recast, introducing the wall units and the definitions of Re_τ and Ra , in the following

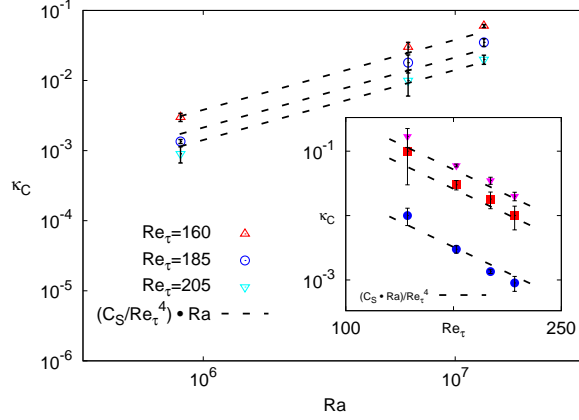


FIGURE 8. Plots of the parameter $\kappa_C(Ra, Re_\tau)$ of the model as function of Ra for fixed Re_τ (main panel) and as function of Re_τ for fixed Ra (inset). The dashed lines represent equation (4.2) with constant C_S fixed at $C_S = 2.5$ for all cases.

form

$$\frac{1}{\kappa y^+} = S^+ \left(1 + C_S \frac{Ra}{Pr^2 Re_\tau^4} y^+ \right); \quad (4.12)$$

it must be noticed that the two parameters κ and C_S are combinations of dimensionless quantities emerging in the derivation, which cannot be, however, derived from first principles; fits of the numerical data indicate that good estimates are the values $\kappa = 0.42$ and $C_S = 2.5$. Explicating the shear term in (4.12), we get

$$\frac{dU^+}{dy^+} = \frac{1}{\kappa y^+ (1 + \kappa C_S y^+)}, \quad (4.13)$$

whose integration finally yields expressions (4.1) and (4.2) for the velocity profile. The robustness of the model is confirmed in Figure 8 where we plot the fitted values of the parameter κ_C as function of Ra for fixed Re_τ (main panel) and as function of Re_τ for fixed Ra (inset), together with the predictions of equation (4.2) (dashed lines).

5. Conclusions

We have studied, by means of direct numerical simulations based on a thermal lattice Boltzmann algorithm, the dynamics of a turbulent channel flow under a gravity field orthogonal to the streamwise direction coupled to an imposed temperature difference between the top (cold) wall and the bottom (hot) wall. The resulting unstably stratified configuration flattens the velocity profile and decreases the centreline value when the buoyancy strength is increased. This effective drag shows up in an enhancement of the friction coefficient. The action of buoyancy on the boundary layer structure has also been probed looking at other relevant statistical quantities in wall bounded turbulent system, such as Reynolds stress; we have found that, as the Rayleigh number is increased, the squared wall normal velocity grows in the bulk becoming comparable or even larger than the streamwise component (which, in turn, is depleted close to the wall). To provide a quantitative interpretation of the numerical findings, we have proposed a phenomenological model resulting in a modified logarithmic law of the boundary layer; such model could successfully capture the various velocity profiles at changing the shear Reynolds and Rayleigh number, with just one adjustable parameter.

AS, HE and AG acknowledge financial support from the Icelandic Research Fund. AS acknowl-

edges funding from the European Research Council under the EU Seventh Framework Programme (FP7/2007-2013) / ERC Grant Agreement no[279004]. This work was partially supported by the Foundation for Fundamental Research on Matter (FOM), a part of the Netherlands Organisation for Scientific Research (NWO), and by the COST action MP1305.

REFERENCES

- AHLERS G., BODENSCHATZ E., FUNFSCHILLING D., GROSSMANN S., HE X., LOHSE D., STEVENS R.J.A.M. & VERZICCO R. 2012 Logarithmic temperature profiles in turbulent Rayleigh-Bénard convection. *Phys. Rev. Lett.* **109**, 114501.
- AIDUN C.K. & CLAUSEN J.R. 2010 Lattice Boltzmann Method for complex flows. *Annu. Rev. Fluid Mech.* **42**, 439-472.
- ARMENIO V. & SARKAR S. 2002 An investigation of stably stratified turbulent channel flow using large-eddy simulation. *J. Fluid Mech.* **459**, 1-42.
- BENZI R., SUCCI S. & VERGASSOLA M. 1992 The lattice Boltzmann equation: theory and applications. *Phys. Rep.* **222**, 145-197.
- BLUESTEIN H.B. 2013 *Severe convective storms and tornadoes*, Springer.
- CHEN S. & DOOLEN G.D. 1998 Lattice Boltzmann Method for fluid flows. *Annu. Rev. Fluid Mech.* **30**, 329-364.
- GARCÍA-VILLALBA M & DEL ÁLAMO J.C 2011 Turbulence modification by stable stratification in channel flow. *Phys. Fluids* **23**, 045104.
- GERZ T., SCHUMANN U. & ELGOBASHI S.E. 1989 Direct numerical simulation of stratified homogeneous turbulent shear flows. *J. Fluid Mech.* **200**, 563-594.
- HATTORI H., MORITA A. & NAGANO Y. 2006 Nonlinear eddy diffusivity models reflecting buoyancy effect for wall-shear flows and heat transfer. *Int. J. Heat Mass Transfer* **27**, 671-683.
- HE X., CHEN S. & DOOLEN G.D. 1998 A novel thermal model for the Lattice Boltzmann Method in incompressible limit. *J. Comp. Phys.* **146**, 282-300.
- IIDA O. & KASAGI N. 1997 Direct numerical simulation of unstably stratified turbulent channel flow. *J. Heat Transfer - Trans. ASME* **119**, 53-61.
- IIDA O., KASAGI N. & NAGANO Y. 2002 Direct numerical simulation of turbulent channel flow under stable density stratification. *Int. J. Heat Mass Transfer* **45**, 1693-1703.
- JOHANSSON A.V. & WIKSTRÖM P.M. 1999 DNS and modelling of passive scalar transport in turbulent channel flow with a focus on scalar dissipation rate modelling. *Flow, Turbulence and Combustion* **63**, 223-245.
- KADER B.A. & YAGLOM A.M. 1990 Mean fields and fluctuations moments in unstably stratified turbulent boundary layers. *J. Fluid Mech.* **212**, 637-662.
- KOMORI S., UEDA H., OGINO F. & MIZUSHINA T. 1982 Turbulence structure in unstably-stratified open-channel flow. *Phys. Fluids* **25**, 1539-1546.
- L'VOV V.S., POMYALOV A., PROCACCIA I. & TIBERKEVICH V. 2004 Drag reduction by polymers in wall bounded turbulence. *Phys. Rev. Lett.* **92**, 244503.
- LUMLEY J.L., ZEMAN O. & SIESS J. 1978 The influence of buoyancy on turbulent transport. *J. Fluid Mech.* **84**, 581-597.
- MONIN A.S. & OBUKHOV A.M. 1954 Basic laws of turbulent mixing in the atmospheric boundary layer *Trudy Inst. Teor. Geofiz. Akad. Nauk SSSR* **24**, 163-187.
- OBUKHOV A.M. 1946 Turbulence in thermally inhomogeneous atmosphere. *Trudy Inst. Teor. Geofiz. Akad. Nauk SSSR* **1**, 95-115.
- PAPAVASSILIOU D.V. & HANRATTY T.J. 1997 Transport of a passive scalar in a turbulent channel flow. *Int. J. Heat Mass Transfer* **40**, 1303-1311.
- POPE S.B. 2001 *Turbulent flows*, Cambridge University Press.
- PRANDTL L. 1932 Meteorologische Anwendung der Strömungslehre. *Beitr. Phys. fr. Atmos.* **19**, 188-202.
- PAPAVASSILIOU D.V. & HANRATTY T.J. 2008 Theory of drag reduction by polymers in wall-bounded turbulence. *Rev. Mod. Phys.* **80**, 225-247.
- SCAGLIARINI A., GYLFASON A., & TOSCHI F. 2014 Heat-flux scaling in turbulent Rayleigh-Bénard convection with an imposed longitudinal wind. *Phys. Rev. E.* **89**, 043012.
- WOLF-GLADROW D. 2001 *Lattice-gas cellular automata and lattice Boltzmann models: An introduction*, Springer.

- BENZI R., TOSCHI F., & TRIPICCIONE R. 1998 On the heat transfer in Rayleigh-Bénard systems. *J. Stat. Phys.* **93**, 901.
- CALZAVARINI E., TOSCHI F., & TRIPICCIONE R. 2002 Evidences of Bolgiano-Obukhov scaling in three-dimensional Rayleigh-Bénard convection. *Phys. Rev. E* **66**, 016304.
- TOSCHI F., AMATI G., SUCCI S., BENZI R. & PIVA R. 1999 Intermittency and structure functions in channel flow turbulence. *Phys. Rev. Lett.* **82**, 5044.
- TOSCHI F., LÉVÊQUE E. & RUIZ-CHAVARRÍA G. 2000 Shear effects in nonhomogeneous turbulence. *Phys. Rev. Lett.* **85**, 1436.
- BIFERALE L., LOHSE D., MAZZITELLI I. & TOSCHI F. 2002 Probing structures in channel flow through SO(3) and SO(2) decomposition. *J. Fluid Mech.* **452**, 39-59.
- LAVEZZO V., CLERCX H.J.H. & TOSCHI F. 2011 Rayleigh-Bénard convection via Lattice Boltzmann method: code validation and grid resolution effects. *J. Phys.: Conf. Ser.* **333**, 012011.
- ZAINALI A. & LESSANI B. 2010 Large-eddy simulations of unstably stratified turbulent channel flow with high temperature differences. *Int. J. Heat Mass Transfer* **53**, 4865-4875.
- ZONTA F., ONORATO M. & SOLDATI A. 2012 Turbulence and internal waves in stably-stratified channel flow with temperature-dependent fluid properties. *J. Fluid Mech.* **697**, 175-203.